Poly(D-amino acid) Nanoparticles Target *Staphylococcal* Growth and Biofilm Disassembly by Interfering with Peptidoglycan Synthesis

Wenli Feng, Marco Chittò, Wensheng Xie, Qun Ren, Fang Liu, Xiaoxu Kang, Dongdong Zhao, Guofeng Li,* Thomas Fintan Moriarty,* and Xing Wang*

Cite This: https://doi.org/10.1021/acsnano.3c10983

Read Online

ACCESS | Metrics & More | Article Recommendations | Supporting Information

ABSTRACT: D-Amino acids are signals for biofilm disassembly. However, unexpected metabolic pathways severely attenuate the utilization of D-amino acids in biofilm disassembly, resulting in unsatisfactory efficiency. Herein, three-dimensional poly(D-amino acid) nanoparticles (NPs), which possess the ability to block intracellular metabolism, are constructed with the aim of disassembling the biofilms. The obtained poly(α-N-acryloyl-D-phenylalanine)-*block*-poly(β-N-acryloyl-D-aminoalanine NPs (denoted as FA NPs) present α-amino groups and α-carboxyl groups of D-aminoalanine on their surface, which guarantees that FA NPs can effectively insert into bacterial peptidoglycan (PG) via the mediation of PG binding protein 4 (PBP4).

Subsequently, the FA NPs trigger the detachment of amyloid-like fibers that connect to the PG and reduce the number of polysaccharides and proteins in extracellular polymeric substances (EPS). Finally, FA NPs damage the structural stability of EPS and lead to the disassembly of the biofilm. Based on this feature, FA NPs significantly enhance the killing efficacy of encapsulated sitafloxacin sesquihydrate (Sita) by facilitating the penetration of Sita within the biofilm, achieving complete elimination of *Staphylococcal* biofilm in mice. Therefore, this study strongly demonstrates that FA NPs can effectively improve biofilm disassembly efficacy and provide great potential for bacterial biofilm infection treatment.

KEYWORDS: poly(D-amino acid) nanoparticles, peptidoglycan binding protein 4, transpeptidation, peptidoglycan insertion, Staphylococcal biofilm disassembly
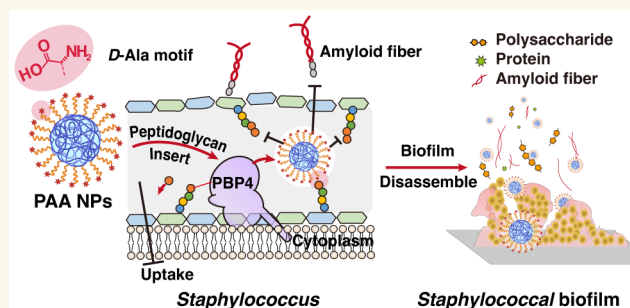
INTRODUCTION

Bacterial biofilm infection is the main cause of implant failure.[1−3] When bacteria adhere to the surfaces of implants, they produce extracellular polymeric substances (EPS) and form a dense structure known as biofilm.[4,5] The biofilm not only protects bacteria from the immune system and limits the penetration of antibiotics but also reduces the bacterial metabolic activity, leading to reduced efficacy of antibiotics.[6−8] As such, bacteria in biofilm are considered highly antibiotic tolerant, even in the absence of antibiotic resistance genes.[9−11]

D-Amino acids (D-AAs), which are generated by bacteria in the stationary phase, are a signal for biofilm disassembly.[12] This provides the opportunity for D-AAs to be used as a natural synergist to improve the efficacy of antibiotics as well as decrease their dosage in eliminating biofilm.[13,14] For example, the D-AAs−vancomycin combination therapy resulted in

higher biofilm clearance in *Staphylococcus aureus* (*S. aureus*)-induced periprosthetic joint infection.[15] Warraich et al. employed D-Asp and D-Glu to promote the elimination efficiency of ciprofloxacin for *S. aureus* biofilms.[16] Nevertheless, it should be noted that D-AAs can not only participate in biofilm disassembly processes like interfering with the function of the bacterial cell wall, regulating the synthesis of protein, and modulating the bacterial mobility and adhesion but also participate in others' metabolism in bacteria, such as L-amino

Scheme 1. Schematic representation of the FA NPs' assembly procedures and functional mechanisms to disassemble biofilm by interfering with the PG synthesis.
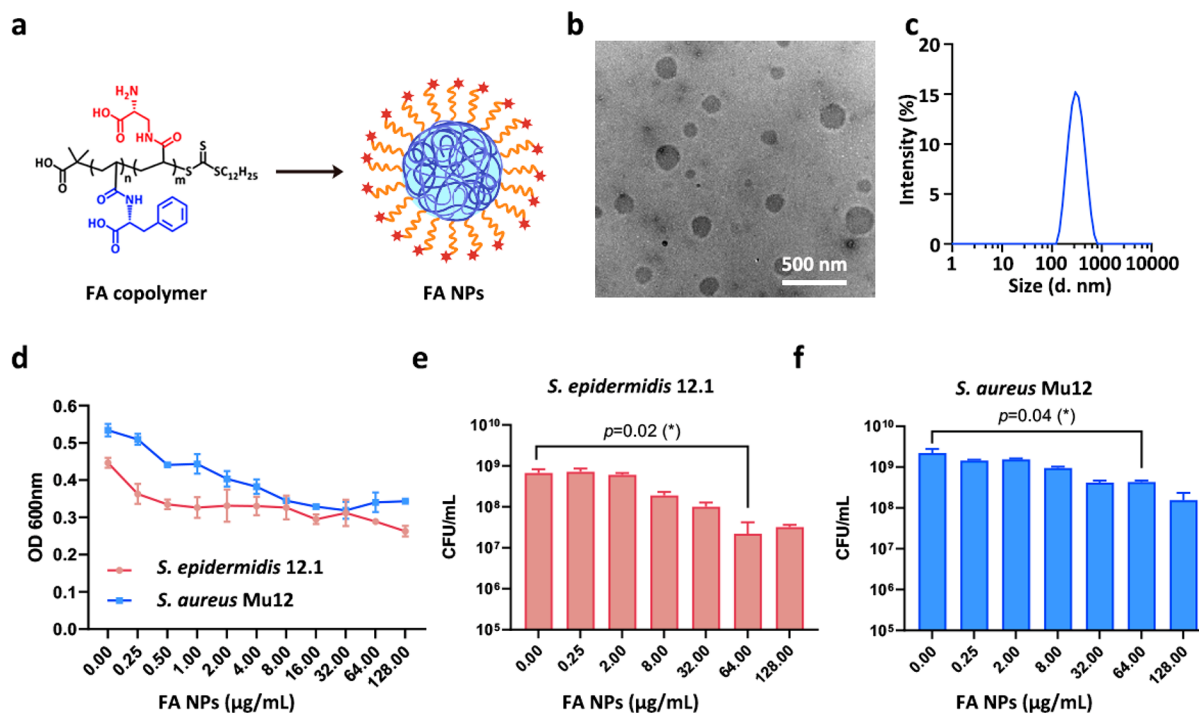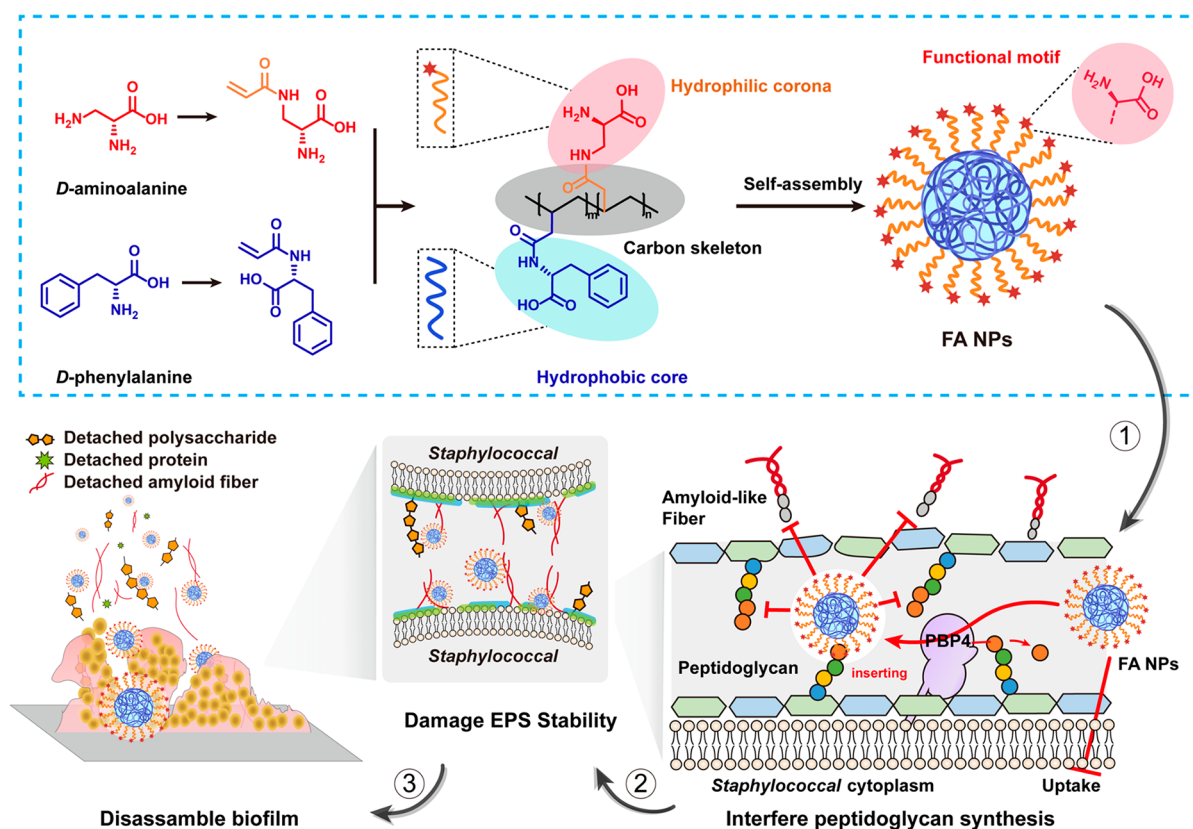

Figure 1. Characteristics of FA NPs. (a) The assembly of FA NPs. (b) TEM images of FA NPs. (c) Size distribution of FA NPs determined by DLS (PDI = 0.169). (d) OD600 of *Staphylococcal* planktonic bacteria after co-incubating with various concentrations of FA NPs in tryptic soy broth medium (TSB, $n = 3$). Corresponding quantified CFU of (e) *S. epidermidis* 12.1 and (f) *S. aureus* Mu12, $n = 3$. Data are expressed as the mean $\pm$ standard deviation (SD), Student's t test, $*p < 0.05$.

acid conversion, phosphate uptake, and the citrate cycle.[17−19] Consequently, only a limited amount of any D-AA will be available for biofilm disassembly. Therefore, efforts have been made to integrate D-AAs into a hydrogel or nanoparticles
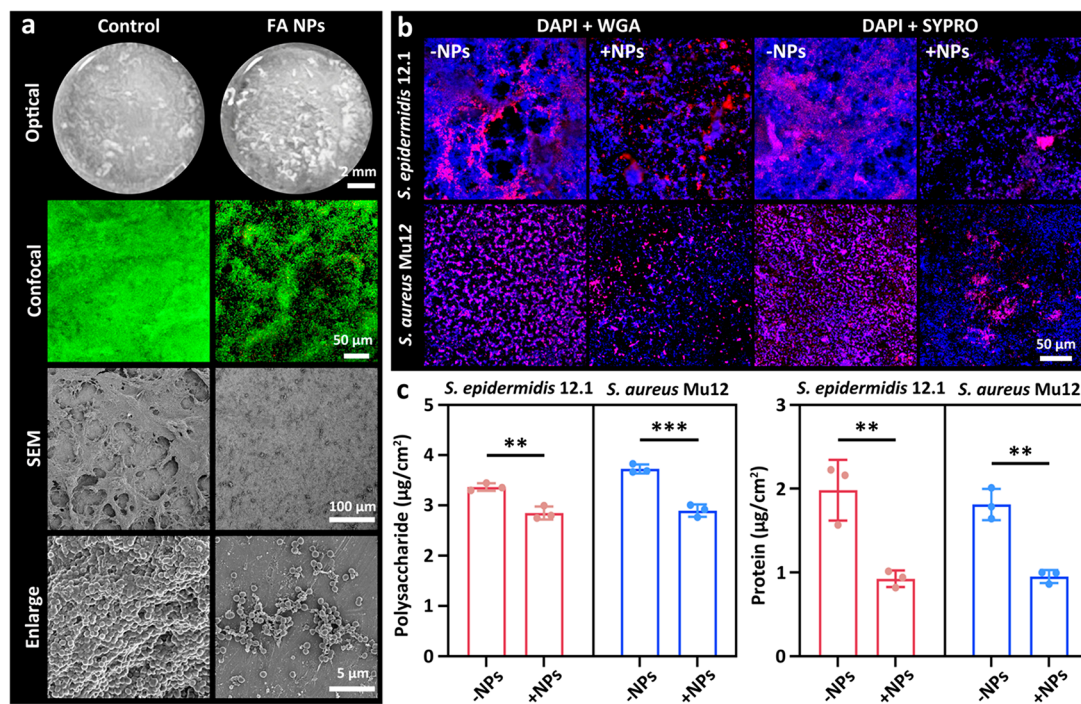
Figure 2. *Staphylococcal* biofilm treatment with/without FA NPs and a relevant change of EPS. (a) The morphology (including bright field, confocal laser scanning microscope (CLSM) images, and SEM images) of the *Staphylococcal* 12.1 biofilm treated with/without FA NPs. For CLSM images, the bacteria were stained using a live/dead kit with Syto9 (green: live) and PI (red: dead). (b) CLSM images of *Staphylococcal* (*S. epidermidis* 12.1 and *S. aureus* Mu12) biofilms with and without FA NP treatment. Biofilms were stained with wheat germ agglutinin (WGA, red for polysaccharides) or FilmTracer SYPRO Ruby (red for proteins), in combination with 4,6-diamino-2-phenylindole (DAPI, blue for nucleic acids), respectively. (c) EPS quantification of the biofilms treated by FA NPs ($n = 3$). Data are expressed as the mean $\pm$ SD, Student's t test, ***$p < 0.001$, **$p < 0.01$.

(NPs) for increasing the local concentration of D-AAs within the biofilm and improve disassembly efficacy.[20,21] Sanchez Jr. et al. used polyurethane scaffolds to deliver mixed D-AAs (1:1:1 of D-Met:D-Pro:D-Trp) for implant biofilm infection treatment.[22] Qu et al. developed a multifunctional nanodevice for spatiotemporally releasing free D-AAs to disperse biofilm.[23] However, limitations of D-AAs still exist because they are used in a small-molecule form. Recently, Chen et al. developed cationic amphiphilic polypeptides that exhibit configuration-dependent inhibition of biofilm formation.[24] But disassembling mature biofilm by using D-AA-based polymers remains elusive and presents a significant challenge. Thus, our hypothesis is that three-dimensional (3D) poly(D-AA) NPs using D-AAs as the building blocks would have the opportunity to increase efficacy in biofilm disassembly, while limiting their unexpected consumption in other metabolic processes.

Herein, to verify our hypothesis, a D-AA-based copolymer, poly(α-N-acryloyl-D-phenylalanine)-*block*-poly(β-N-acryloyl-D-aminoalanine) (denoted as FA), which consists of poly(α-N-acryloyl-D-phenylalanine) (PF) as a hydrophobic core and poly(β-N-acryloyl-D-aminoalanine) (PA) as the hydrophilic corona, was synthesized and further assembled into NPs (denoted as FA NPs) (Scheme 1). The 3D structure endowed FA NPs with numerous advantages: (i) The carbon skeleton of FA NPs greatly provided structural stability by avoiding enzymatic degradation and significantly blocking unexpected primary metabolism of D-AAs from FA NPs. (ii) The polymeric pendant structure effectively preserved the α-amino groups and α-carboxyl groups of D-aminoalanine, which guaranteed the ability of FA NPs for bacterial targeting and might have the potential for interfering with the function

of the bacterial cell wall. Consequently, the FA NPs specifically inserted into PGs via PG binding protein 4 (PBP4) mediation. The inserted FA NPs in PGs further triggered the detachment of amyloid-like fibers that connected with PGs and reduced the number of polysaccharides and proteins in EPS. Thereby, FA NPs damaged the structural stability of EPS and led to the disassembly of biofilm. This study strongly demonstrated that FA NPs could exert the properties of D-AAs, effectively promoting the disassembly of biofilms. Furthermore, FA NPs significantly enhanced the susceptibility to antibiotic killing, achieving complete elimination of the biofilm in mice. Overall, FA NPs possess great potential for bacterial biofilm infection treatment.

RESULTS AND DISCUSSION

The FA copolymer was synthesized via photoinduced electron/energy transfer—reversible addition—fragmentation chain-transfer (PET-RAFT) polymerization[25] (Scheme S1). The molecular weight of FA was calculated to be 9569 g/mol, while the polymerization degrees of PF and PA were 29 and 18, respectively (Figurea S1—S3, Table S1). To assemble FA NPs with good morphology and narrow size distribution, FA NPs were prepared via self-assembly in a mixed solvent system of DMSO/water (1/9, v/v) (Figure 1a). Transmission electron microscopy (TEM) images (Figure 1b) showed the spherical structure of as-synthesized FA NPs with a narrow size distribution of approximately 175 ± 7 nm, which was further confirmed by the results of dynamic light scattering (DLS) (Figure 1c). The impact of FA NPs on planktonic bacteria was assessed. As shown in Figure 1d, the growth of planktonic bacteria was suppressed when increasing the addition of FA
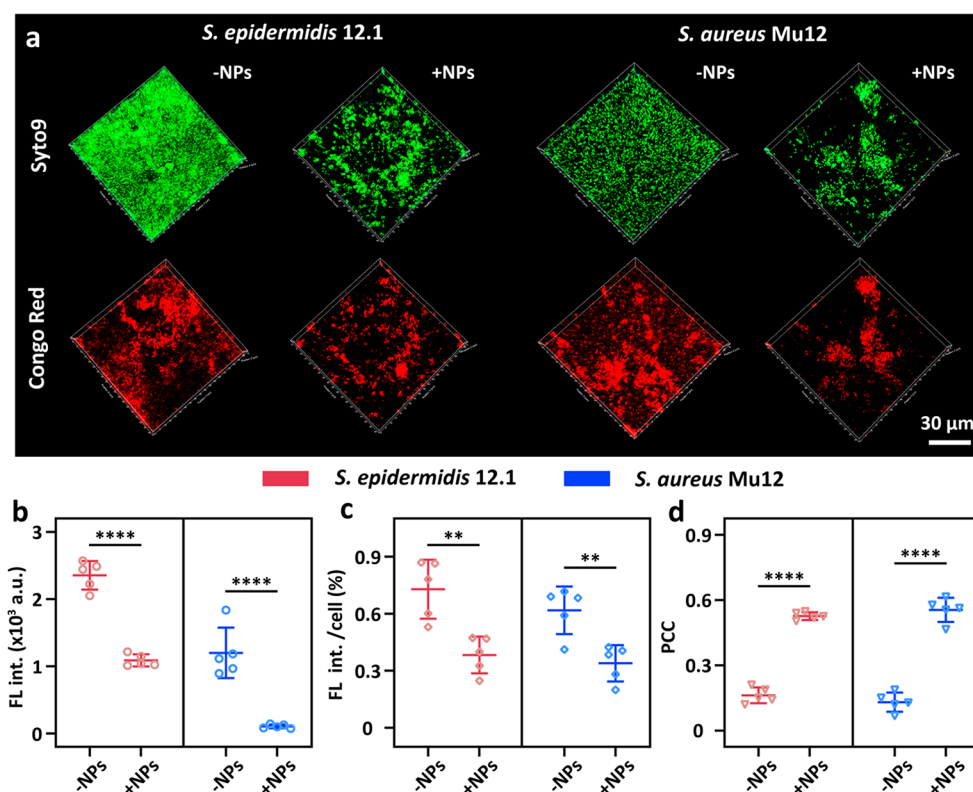
Figure 3. Influence on amyloid-like fiber components of *Staphylococcal* biofilms treated with FA NPs. (a) CLSM images of *Staphylococcus* biofilms with/without FA NP treatment. The live bacterial cells of the biofilm and the amyloid-like fibers were stained using Syto9 (green) and Congo Red (red), respectively. (b) The total red fluorescent intensity (FL int.) of amyloid-like fibers in treated biofilms. (c) Normalized fibril fluorescent intensity of bacteria from treated biofilms. (d) Co-localization Pearson's coefficient (PCC) of the bacteria and amyloid-like fibers, respectively ($n = 5$). Data are expressed as the mean $\pm$ SD, Student's t test, ****$p < 0.0001$, **$p < 0.01$.

NPs. Colony forming unit (CFU) counting (Figure 1e,f) displayed that those high concentrations (>64 μg mL^{-1}) of FA NPs decreased the bacterial density to approximately 1 log$_{10}$CFU ($p = 0.01$ for *Staphylococcus epidermidis* (*S. epidermidis*) 12.1; $p = 0.04$ for *S. aureus* Mu12), indicating that high concentrations of FA NPs might possess slight bactericidal ability.

Subsequently, the biofilm disassembly ability of FA NPs was examined (Figure 2). In the untreated biofilm, optical, confocal fluorescence, and scanning electron microscope (SEM) images clearly showed that *S. epidermidis* 12.1 could form a strong and dense biofilm with an even surface distribution (Figure 2a), and D-alanine exhibited a negligible biofilm disassembly effect (Figure S4). In contrast, after treatment with FA NPs, *S. epidermidis* 12.1 biofilm was apparently disassembled with an irregular or uneven surface distribution, confirmed by fluorescence images, which showed a disrupted internal structure. Co-localization studies of the *S. epidermidis* 12.1 biofilm treated with FA NPs (Figure S5) revealed that FA NPs were able to effectively penetrate the biofilm, apparently disrupting its structural integrity and generating a large number of channels or voids in the biofilm. This effect of FA NPs was universal and could be exerted when treating *S. aureus* Mu12 biofilm (Figure S5). Measurement of the defect area (namely, gap area) of the biofilm with FA NP treatment was significantly larger than that without FA NP treatment (Figure S6). Interestingly, in SEM observation, the *S. epidermidis* 12.1 biofilm treated with FA NPs was completely disassembled, and only sporadic colonies were visible, which was extremely different from the untreated biofilm (Figure 2a). Possibly, the

FA NPs were disassembling the biofilm, and the washing steps for SEM preparation removed the detached biofilm portion. This variation strongly implied that the biofilm structural strength was destroyed by FA NPs.

Notably, the bactericidal activity of FA NPs was limited and did not damage the biofilm to a large extent. Therefore, the direct damage of EPS would contribute to the biofilm disassembly.[26,27] Accordingly, confocal laser scanning microscope (CLSM) observation and quantification analysis of polysaccharides (stained with wheat germ agglutinin, WGA) and proteins (stained with SYPRO), which are two main macromolecules contributing to EPS, were conducted (Figure 2b,c). CLSM images showed that the fluorescence intensity of polysaccharides and proteins decreased after the FA NP treatment (Figure 2b). Quantification analysis (Figure 2c, Figure S7) further demonstrated that their amount in *S. epidermidis* 12.1, *S. aureus* Mu12, and *S. aureus* ATCC 6538p biofilms decreased significantly, suggesting the biofilm disassembly mediated by FA NPs.

In addition to proteins and polysaccharides, amyloid-like fibers are also the key component of EPS in *Staphylococcal* biofilm.[28,29] These amyloid-like fibers are tightly anchored to the cell wall and form stable scaffolds, which will fix the cell together and aid in processes of bacterial adhesion, aggregation, and biofilm formation.[30,31] Therefore, we examined the change of amyloid-like fibers in biofilm with/without FA NP treatment using Congo Red staining.[32] As shown in Figure 3a, both *Staphylococcal* biofilms had a significant number of amyloid-like fibers (dense red fluorescence). However, the number of amyloid-like fibers
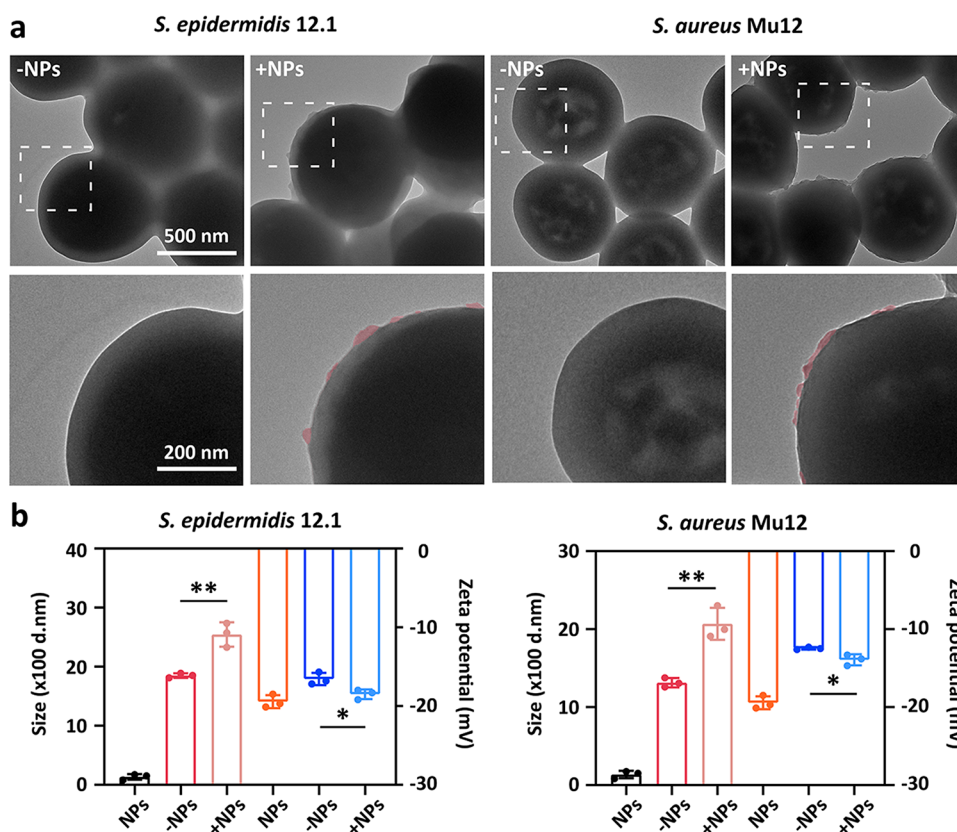
Figure 4. Study on the binding behaviors of FA NPs on *Staphylococcal* planktonic bacteria. (a) TEM images of planktonic bacteria cultured in TSB medium with/without FA NP treatments. The bottom images are the magnified view of the selected regions. The red color indicates the FA NPs. (b) Corresponding hydrodynamic diameter and zeta potentials of bacteria after different treatment exposure ($n = 3$). Data are expressed as the mean $\pm$ SD, Student's t test, **$p < 0.01$, *$p < 0.05$.

decreased noticeably after treatment with FA NPs. Consistently, a 1.27-fold (for *S. epidermidis* 12.1 biofilm) and 1.09-fold (for *S. aureus* Mu12 biofilm) decrease in mean fluorescence intensity of amyloid-like fibers for the FA NP group was observed compared with the control group (Figure 3b). This implied that FA NPs destroyed the structural integrity and stability of the biofilm. In order to study the ratio changes between amyloid-like fibers to other components in biofilms, we standardized the fluorescence intensity of amyloid-like fibers using that of bacteria as a benchmark. Interestingly, the result showed that the normalized fluorescence intensity of amyloid-like fibers exhibited an obvious decrease (Figure 3c), which demonstrated that the decrease of amyloid-like fibers was more than that of bacteria in the biofilm after treatment with FA NPs. It suggested that the damage to the structural stability of amyloid-like fibers might be the main contributor to the disassembly of *Staphylococcal* biofilms. Moreover, the co-localization of the remaining amyloid-like fibers with bacteria (Figure 3d) was significantly enhanced, demonstrating that the remaining amyloid-like fibers were mainly present on the surface of bacteria. These results revealed that FA NP treatment mainly damaged the structural stability and reduced the number of amyloid-like fibers connecting between bacteria. Subsequently, the weaker connection between bacteria made the biofilm more fragile, finally leading to biofilm disassembly.

It has previously been shown that amyloid-like fibers are mainly bound to the surface of the bacterial cell wall.[33] So we speculate that FA NPs damage the connection between the amyloid-like fibers and bacteria via an interaction with bacterial surface structures. As shown in Figure 4a, both *S. epidermidis* 12.1 and *S. aureus* Mu12 presented smooth surfaces, which became rough after treatment with FA NPs for 6 h. This implied that FA NPs could efficiently anchor to the surface of *Staphylococci*. The zeta potential of the bacteria was significantly reduced ($p < 0.05$) after FA NP treatment in TSB medium, further demonstrating that FA NPs could bind to the surface of the bacterial cell wall. Interestingly, we noticed that the size of *Staphylococci* noticeably increased by 37−57% after FA NP treatment (Figure 4b). Therefore, we speculate that the change not only is caused by the surface binding of FA NPs but also may contribute to the inhibition of bacterial proliferation by FA NPs.[34,35] To investigate this, planktonic bacteria were kept in a phosphate-buffered solution (PBS) solution, where the growth and proliferation would be decelerated, and further treated with FA NPs. The results (Figure S8) revealed that there was no significant change in the size and zeta potential of the bacteria, demonstrating that FA NPs could specifically bind to the bacterial surface when the bacteria were actively dividing. Therefore, it could be concluded that the interaction between FA NPs and the bacterial surface was not through nonspecific interactions such as conventional electrostatic adsorption or hydrogen-bonding interaction, but rather via the specific binding process during the bacterial growth.

During the growth and proliferation period, exogenous D-AAs can specifically insert into the PG on the *Staphylococcal* cell walls,[36−38] which can interfere with the binding ability between amyloid-like fibers and the cell wall.[39] But, whether
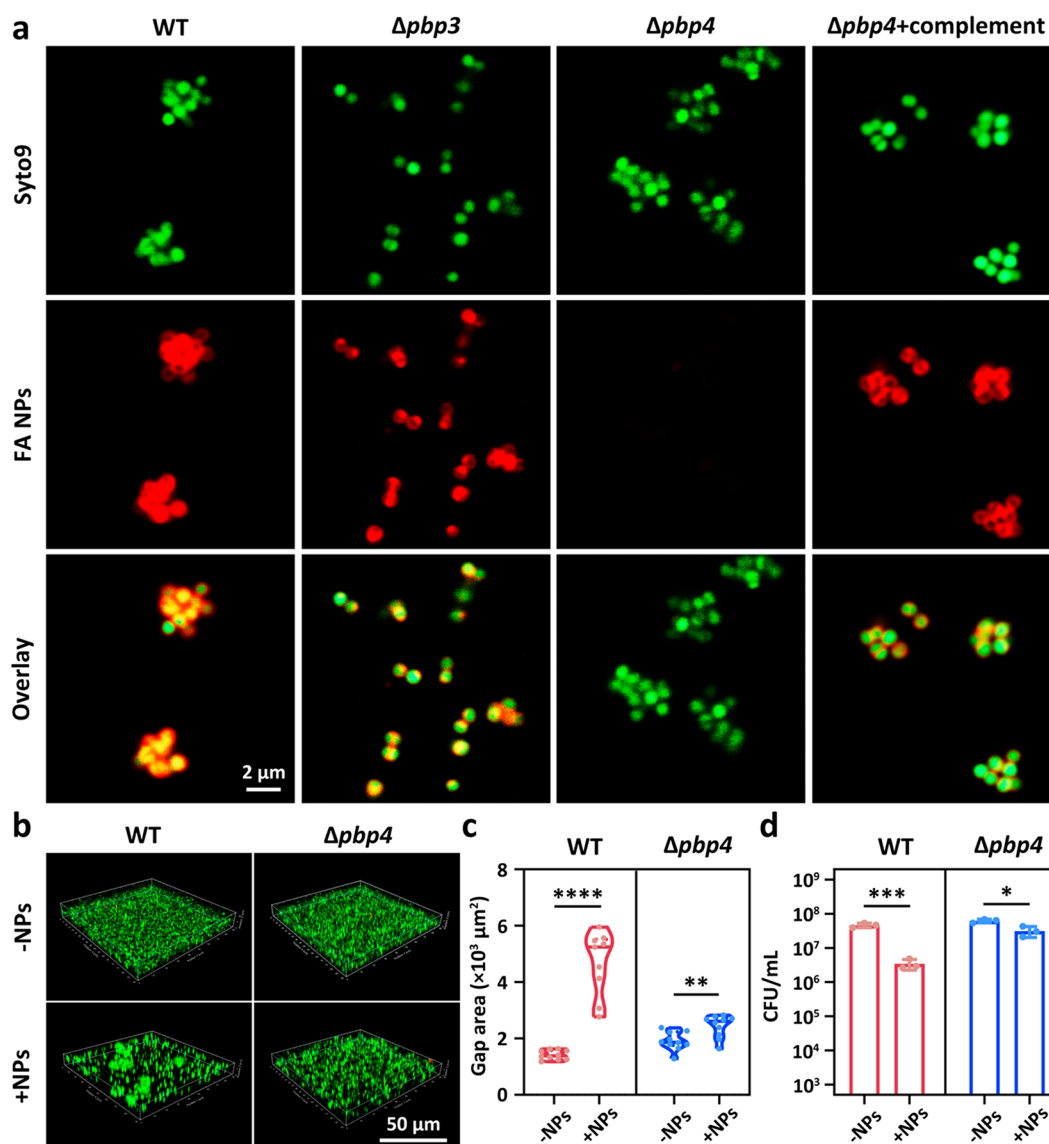
Figure 5. Mechanism of FA NPs inserting PG mediated by PBP4 protein. (a) CLSM images of wild-type (WT) and mutant ($\Delta pbp3$, $\Delta pbp4$, $\Delta pbp4$+complement) *S. aureus* USA300 planktonic bacteria co-incubated with NR@FA NPs, and the bacteria were stained with Syto9 (green). (b) Confocal z-stack images of WT and $\Delta pbp4$ USA300 biofilms without/with FA NPs in a TSB medium. The biofilms were stained with a bacterial Live/Dead kit, Syto9 (green: live), and PI (red: dead). (c) Respective gap area calculated from confocal images ($n = 10$). (d) The surviving bacterial counts in treated biofilms ($n = 3$). Data are expressed as the mean $\pm$ SD. Student's *t* test, ****$p < 0.0001$, ***$p < 0.001$, **$p < 0.01$, *$p < 0.05$.

FA NPs, as large-scale 3D poly(D-AAs) NPs, can be inserted into PG following the same pathway is still unknown. To address this question, wild type (WT) and mutant strain ($\Delta pbp3$ and $\Delta pbp4$) *S. aureus* USA300 were chosen to investigate the specific interaction between FA NPs and bacteria. As shown in Figure 5a, the bright yellow fluorescence for the WT *S. aureus* USA300 indicated good co-localization between the FA NPs with Nile Red loading (denoted as NR@ FA NPs, red fluorescence) and WT *S. aureus* USA300 (green fluorescence).

In addition, the co-incubation of FA NPs with the $\Delta pbp3$ mutant strain also showed good co-localization, demonstrating that the PBP3 protein did not interact with FA NPs. Interestingly, when the *pbp4* gene of *S. aureus* USA300 was knocked out, the insertion ability of FA NPs into PG was lost. No red fluorescence was observed on the surface of $\Delta pbp4$ *S. aureus* USA300 (Figures 5a and S9). Meanwhile, the surface

morphology, zeta potential, and size of $\Delta pbp4$ *S. aureus* USA300 did not show significant change after FA NP treatment (Figure S10). These results suggested that FA NPs were highly likely to be inserted into the PG of *S. aureus* USA300 through mediation of the PBP4 protein. To further prove this judgment, the complement strain was used to recover the function of PBP4 protein in $\Delta pbp4$ *S. aureus* USA300 (denoted as $\Delta pbp4$+complement *S. aureus* USA300) together with FA NPs. It was found that when PBP4 function was restored, the FA NPs were able to retarget $\Delta pbp4$+complement *S. aureus* USA300, showing strong complex yellow fluorescence (Figure 5a), which was comparable to the effect of WT *S. aureus* USA300. Additionally, the co-localization between the peptidoglycan and FA NPs was evaluated.[40,41] CLSM images (Figure S11) clearly showed the strong co-localization effect between NR@FA NPs in red fluorescence and peptidoglycan in green fluorescence,
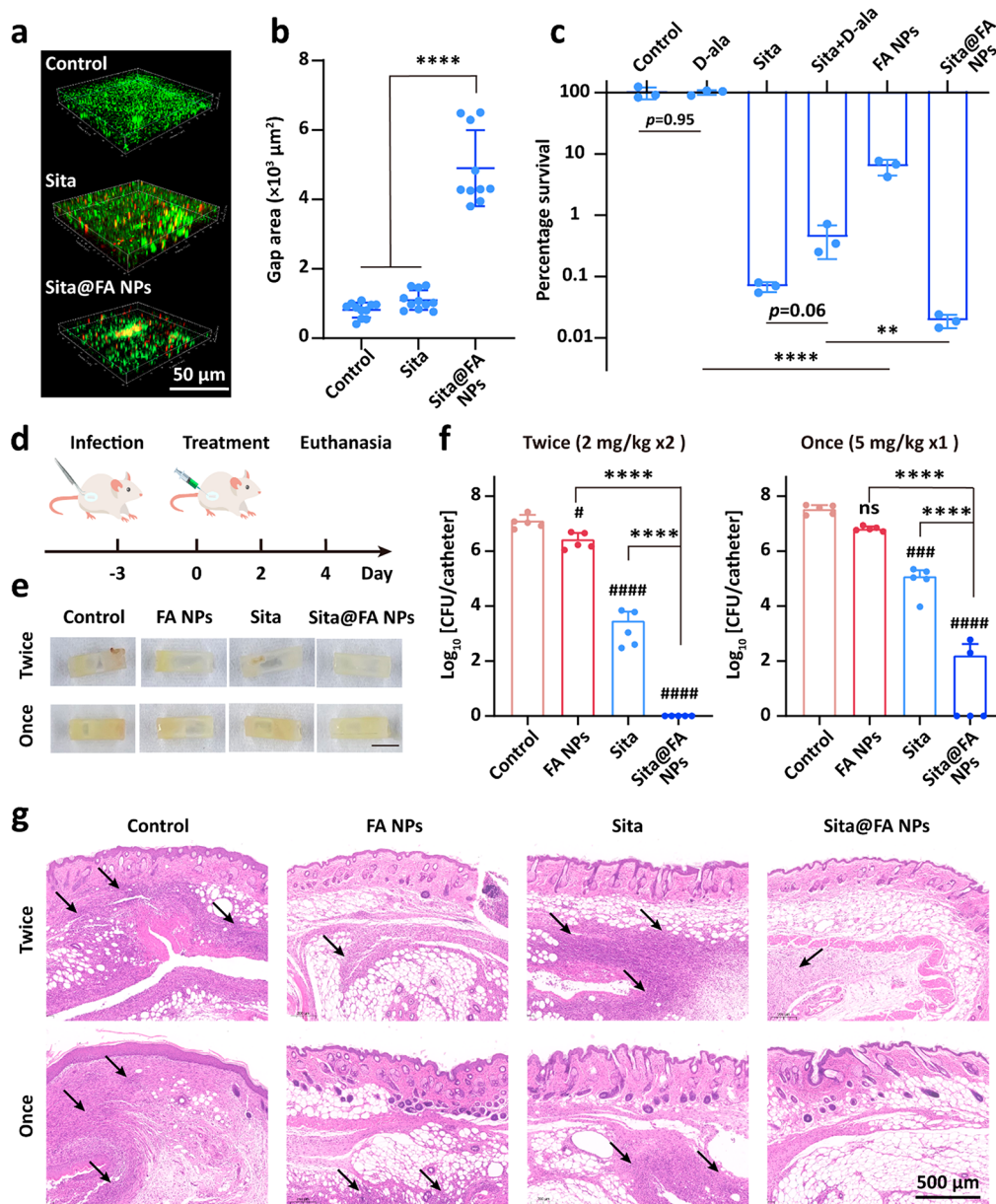
Figure 6. *In vitro* and *in vivo* evaluation of the *Staphylococcal* biofilm elimination ability of FA NPs and Sita-loaded NPs (Sita@FA NPs). (a) Confocal z-stack images of the *S. aureus* Mu12 biofilm treated with TSB, FA NPs, and Sita@FA NPs. The biofilms were stained with a bacterial Live/Dead kit, Syto9 (green: live), and PI (red: dead). (b) Respective gap area of differently treated biofilms ($n = 11$), one-way ANOVA test. (c) Corresponding viability of bacteria in biofilm after various treatments ($n = 3$). Student's t test. (d) Schematical illustration of the *in vivo* study plan. "Once" and "Twice" stand for single administration (5 mg/kg Sita) and two times the administration (2 mg/kg Sita each time), respectively. (e) The photos of explanted catheters from mice after different treatments. The scale bar is 0.5 cm. (f) Quantification analysis of remaining bacteria from catheters after different treatments ($n = 5$). (g) H&E-stained images of the wound tissues at the implanted sites after the different treatments. The black arrows indicate the inflammatory cell infiltration. One-way ANOVA with the Tukey test. Data are expressed as the mean ± SD, ****$p < 0.0001$, **$p < 0.01$, *$p < 0.05$.

suggesting their excellent targeting ability on peptidoglycan. The peptidoglycan-targeting effect of FA NPs was further studied using two small-molecule inhibitors, vancomycin and flavomycin.[42,43] As shown in Figure S12, the mean fluorescence intensity of bacteria treated with NR@FA, as measured by flow cytometry, was normalized to 100%. Conversely, the mean fluorescence intensity of bacteria treated by NR@FA NPs supplemented with vancomycin, which is a transpeptidation inhibitor, exhibited a significant decrease of approximately 40% ($p = 0.0005$ and 0.0004 for 0.25× minimum inhibitory concentrations (MIC) and 0.5× MIC,

respectively). This implied that the incorporation of NR@FA NPs was mediated mainly by the transpeptidation of PBP4. Comparatively, the mean fluorescence intensity of bacteria treated by NR@FA NPs supplemented with flavomycin, a transglycosylation inhibitor, showed a negligible effect ($p = 0.63$) on the insertion of NR@FA NPs under the low concentration (0.25× MIC), while increasing the concentration to be 0.5× MIC, peptidoglycan formation could be inhibited, which consequently blocked the incorporation of NR@FA NPs in peptidoglycan. Therefore, it fully demon-

strated that these 3D FA NPs were able to specifically insert into the PG of *Staphylococcal* through the mediation of PBP4.

Subsequently, we used WT and mutant (Δ*pbp3*, Δ*pbp4*, Δ*pbp4*+complement) *S. aureus* USA300 to further validate whether the *Staphylococcal* PG insertion by FA NPs would damage the structural integrity of the amyloid-like fibers and finally lead to biofilm disassembly. Confocal z-stack fluorescence images showed that all of the *S. aureus* USA300 strains could form relatively dense biofilms (Figure 5b and Figure S13a). FA NPs could effectively disrupt the biofilms of both WT and Δ*pbp3 S. aureus* USA300. Comparatively, the FA NP treatment caused negligible damage to the Δ*pbp4 S. aureus* USA300 biofilm, revealing that the integration of FA NPs into PG mediated by PBP4 actively participates in the biofilm disassembly process. The difference in the gaps within the biofilm (Figure 5c and Figure S13b) further confirmed the disassembly of the WT and Δ*pbp3 S. aureus* USA300 biofilm, but not the Δ*pbp4* biofilm. In addition, the FA NP treatment led to a decrease of approximately $0.8-1 \log_{10}$CFU in the number of viable bacteria within the WT and Δ*pbp3 S. aureus* USA300 biofilm, whereas the reduction was less than 0.5 $\log_{10}$CFU for the Δ*pbp4 S. aureus* USA300 biofilm (Figure 5d and Figure S13c). Interestingly, when recovering the function of PBP4 protein in Δ*pbp4 S. aureus* USA300 (Δ*pbp4*+complement), the ability of FA NPs to break the biofilm could be recovered and resulted in a similar result to that in the WT *S. aureus* USA300 biofilm (Figure S13). Therefore, it strongly confirmed that PBP4 played a key role in mediating the insertion of exogenous FA NPs into the PG of *Staphylococci*, which then resulted in damaging the structure integrity of EPS and finally led to biofilm disassembly.

Based on the biofilm disassembly mediated by FA NPs, we next investigated whether this would enhance the susceptibility to antibiotic killing. Accordingly, sitafloxacin sesquihydrate (Sita), a type of fluoroquinolone antibiotic, was encapsulated into FA NPs during the self-assembly process to obtain drug-loaded NPs (denoted as Sita@FA NPs) (Figure S14 and Table S2). Both *in vitro* and *in vivo* biofilm elimination efficacy of Sita@FA NPs were then evaluated (Figure 6). Compared with free Sita, Sita@FA NPs were able to disassemble the *S. aureus* biofilm more thoroughly and caused a larger gap area within the biofilm (Figure 6a,b, Figures S15 and S16). CFU results further showed that Sita@FA NPs had the highest elimination efficiency of more than 90% for *Staphylococci* in the biofilm (Figure 6c, Figure S16). The corresponding SEM images also indicated that Sita@FA NPs outperformed free Sita in the treatment of the *Staphylococcal* biofilm (Figure S17). In addition, Sita@FA NPs exhibited a more efficient elimination of bacteria compared to the combined formulation of Sita and D-alanine (denoted as Sita+D-ala), which confirmed that FA NPs enhanced the killing effect of Sita via biofilm disassembly.

Subsequently, an *in vivo* catheter biofilm infection model[44,45] was established in mice to evaluate the *in vivo* biofilm elimination efficacy of Sita@FA NPs. Specifically, the catheter (1 cm in length) with an adhering biofilm was implanted in the inner thighs of mice (Figure 6d). These mice were divided randomly into four groups: FA NP treatment group, Sita treatment group, Sita@FA NP treatment group, and control group. As shown in Figure 6e,f, the antibiotic Sita reduced the total bacterial count by approximately 3 $\log_{10}$CFU after two times of administration (2 mg/kg Sita each time), whereas Sita@FA NPs could completely remove the biofilm with no detectable bacteria found (from >7 $\log_{10}$CFU of the control to

0). The significant killing efficiency within the biofilm strongly suggested that the effect of FA NPs in disassembling the biofilm was very potent for improving the efficiency of antibiotic therapy.

In addition, considering that clinical treatment goals may include reducing the duration of therapy to minimize patient burden, a more challenging single administration mode was carried out to evaluate the elimination effect of Sita@FA NPs. The animals that received one single administration of Sita@FA NPs (5 mg/kg Sita) exhibited superior biofilm elimination efficiency with an extremely low bacterial count (2 $\log_{10}$CFU), while the bacterial count in the Sita group was up to 5 $\log_{10}$CUF (Figure 6f). In addition, skin tissues near the catheter were collected and evaluated by histological staining (H&E) to assess the inflammatory response after treatment (Figure 6g). Compared to the control group, FA NPs and Sita, Sita@FA NPs treatment notably reduced inflammatory cell infiltration and host cell inflammation. Overall, both *in vitro* and *in vivo* results verified that the biofilm disassembly property of FA NPs could effectively improve the elimination efficiency of antibiotics.

CONCLUSION

In summary, a D-AAs-based copolymer was successfully designed and assembled into 3D FA NPs for biofilm disassembly. PBP4 protein plays a key role in mediating the PG-inserting process of FA NPs. The inserted FA NPs in PG further triggered the detachment of amyloid-like fibers that connected with PGs, and reduced polysaccharides and proteins in EPS. Consequently, FA NPs disassembled biofilm by damaging the structural stability of EPS. Due to the 3D structure and special functional groups on the surface, FA NPs could further facilitate the susceptibility to antibiotic killing and finally improve the biofilm elimination efficiency. Both *in vitro* and *in vivo* evaluations demonstrated the superior *Staphylococcal* biofilm elimination performance of Sita@FA NPs compared with that of free Sita. Thus, this study provides a great potential poly(D-AA) for bacterial biofilm infection treatment via biofilm disassembly to improve the elimination efficiency of antibiotics.

EXPERIMENTAL METHODS

Materials and Characterization. D-Phenylalanine, *α-Boc-D-*aminoalanine, and acryloyl chloride were obtained from the Tokyo Chemical Industry (TCI, Japan). Dimethyl sulfoxide (DMSO), dichloromethane (DCM), 2-(dodecylthiocarbonothioylthio)-2-methylpropionic acid (DDMAT), tris(2-phenylpyridine) iridium(III) (Ir(ppy)$_3$), Sita, the LIVE/DEAD BacLight bacterial viability kit, FilmTracer SYPRO Ruby biofilm matrix stain, WGA, Congo Red, PBS, TSB, tryptose soy agar (TSA), and ethanol were purchased from Sigma-Aldrich (USA). DAPI and NR were obtained from Solarbio Science and Technology Co., Ltd. (China). Fixation buffer was purchased from BioLegend (USA).

^{1}H NMR spectra were recorded on a Bruker 400 spectrometer in DMSO-d_6 at 25 °C. The number (M_n)- and weight (M_w)-average molecular weight and polydispersity index (PDI) were determined using a gel permeation chromatography (GPC) equipped with a Waters 2414 refractive index detector, 515 high-performance liquid chromatography (HPLC) pump, and three consecutive Styragel columns (HR1, HR2, and HR4). The eluent was tetrahydrofuran (THF) with a flow rate of 1 mL min^{-1}. The molecular weights were calibrated with polystyrene standards. Prior to GPC analysis, polymers containing a free carboxylic acid functionality underwent methylation using TMSCHN$_2$.

The morphologies of the NPs and bacteria were visualized by TEM (HT-7700, Hitachi, Japan) and SEM (S4700, Hitachi, Tokyo, Japan). The sizes and zeta potential of the NPs and bacteria were studied by DLS (ZetaSizer Nano ZS90, Malvern Instruments, USA). Stained samples were imaged with a CLSM (Zeiss, LSM800, Germany), and images are processed using ZEN (blue edition) software.

The concentration of Sita was analyzed by HPLC (Agilent 1260, USA) with a C18 column (Kinetex 5 μm-C18, 150 mm × 4.6 mm, 100 Å, pH stability 1.5−8.5). The mobile phase consisted of a mixture of KH_2PO_4 (0.05 mol L^{-1}, pH = 2.4) and acetonitrile in a ratio of 70:30 (v/v). The measurements were performed at 25 °C with a flow rate of 1 mL min^{-1} and an injection volume of 10 μL with detection at 295 nm.

Fabrication and Characterization of Copolymer. The monomers, α-N-acryloyl-D-phenylalanine (denoted as F) and β-N-acryloyl-α-Boc-D-aminoalanine (denoted as A_{Boc}), were synthesized according to our previous work.[46] PF was synthesized by using PET-RAFT polymerization. Briefly, F (1 g, 4.56 mmol), DDMAT (33 mg, 0.09 mmol), and $Ir(ppy)_3$ (30 μg, 4.56 × 10^{-5} mmol) were dissolved into 2 mL of DMSO. Then, the mixture was degassed for 30 min to remove the oxygen and reacted for another 6 h under blue light irradiation to obtain PF. Then PF was used to synthesize FA_{Boc} as macro-CTA. Typically, monomer A_{Boc} (1 g, 3.87 mmol), PF (1.3 g, 0.19 mmol), and $Ir(ppy)_3$ (25 μg, 3.87 × 10^{-5} mmol) were dissolved into 1 mL of DMSO. Then, the mixture was degassed for 30 min by N_2 and reacted for 6 h under blue light irradiation. FA was synthesized by detachment of Boc-groups in FA_{Boc}. Generally, 0.1 g of FA_{Boc} was added into 10 mL of DCM and stirred for 10 min. Then, 0.5 mL of TFA was added drop-wisely to the mixture under an ice−water bath. The system was stirred for 3 h at room temperature. All polymers were purified by dialysis against ethanol for 48 h and then dried under a vacuum oven for 12 h. The molecular structure and weight were analyzed by ^{1}H NMR and GPC, respectively.

Preparation of Blank and Sita-Loaded FA NPs. Taking FA NPs as an example, 10 mg of FA polymer was dissolved in 1 mL of DMSO, and then 9 mL of Milli-Q water was added under stirring for self-assembly. The mixture was put into a dialysis bag against Milli-Q water for 48 h to obtain the FA NPs. Similarly, 10 mg of FA polymer and 0.5 mg of Sita were added to form Sita@FA NPs.

Drug Loading and Encapsulating Efficiency. HPLC was employed to measure the concentration of Sita. The loading and encapsulation efficiencies were calculated according to the following format:

Loading content (LC) = (weight of Sita in Sita@FA NPs/weight of Sita@FA NPs) × 100

Encapsulating efficiency (EE) = (weight of Sita in Sita@FA NPs/ weight of used Sita) × 100

Bacterial Strains. Seven Staphylococcus strains were used in this study, including S. epidermidis 12.1, S. aureus Mu12, S. aureus USA300 strains (WT, mutant strain ($\Delta pbp3$, $\Delta pbp4$, $\Delta pbp4$+complement)), and S. aureus ATCC 6538p. TSB was used to culture all of the bacteria. The bacterial inoculation density was 1 × 10^7 CFU mL^{-1}.

In Vitro Biofilm Model. The biofilm model was established on titanium discs in a 48-well plate. The titanium discs were manufactured from medical grade titanium alloy TAN (ISO 5832/11), and the size was 13 mm in diameter and 1 mm thick (surface area 1.33 cm^2). Before use, all disks were washed, air-dried, packed, and sterilized in an autoclave at 121 °C for 20 min. In brief, sterile titanium discs were placed in a 48-well plate. Then, 100 μL of bacteria suspension (OD = 0.1) and 900 μL of sterile TSB were added to each well. The plate was incubated for 24 h at 37 °C in an incubator; 24 h later, fresh sterile TSB with/without FA NPs (250 μg/mL) was used to replace the old medium. Another 24 h later, an in vitro biofilm model was obtained for further use. The obtained biofilm was co-incubated with different agents for 24 h, and CFU, SEM, and CLSM observations were employed for analysis as follows:

CFU Counting. The biofilm was homogenized by ultrasound (200 W, 40 kHz) for 10 min, and CFU counts of the homogeneous solutions were evaluated by performing serial dilutions and plating 10 μL streaks onto TSA plates.

SEM Observation. The biofilm samples were fixed and dehydrated with an ethanol gradient series: 50%, 60%, 70%, 80%, 90%, 96%, and 100% ethanol aqueous solution for 10 min each time. Samples were dried and sputter-coated with 10 nm thick gold/palladium (80:20) using a BAL-TEC MED 020 instrument (BAL-TEC AG, Pfaeffikon, Switzerland) for SEM observation.

CLSM Observation. The biofilm samples were stained respectively with LIVE/DEAD BacLight bacterial viability kit, FilmTracer SYPRO Ruby biofilm matrix stain, WGA, and Congo Red according to the guidelines of the manufacturer. And visualized images were obtained by CLSM.

EPS Extraction and Quantification. The EPS quantification was performed according to the methodology outlined in the literature.[44] Briefly, mature biofilms on titanium disk (surface area 1.33 cm^2) were co-incubated without or with FA NPs (250 μg/mL in TSB) for 24 h. After that, the biofilms were washed with PBS and carefully transferred to a 5 mL tube. Then, the EPS was extracted by ultrasonication and vortexing intermittently (60 W, 30 min in total) in PBS and centrifugation (11000g, 45 min). The supernatant was filtered through a 0.22 μm membrane. The purified EPS was lyophilized and resuspended in distilled water (100 μL). For polysaccharide testing, 90 μL of the exacted EPS sample was mixed with 90 μL of 5% phenol solution and 300 μL of sulfuric acid. The mixture was incubated in a water bath at 90 °C for 1 h, and the absorbance at 490 nm was measured. Glucose was used to create the standard curve. For protein testing, the protein concentration was measured using BCA assay kits in accordance with the manufacturer's guidelines. The contents of polysaccharides and protein in the treated biofilm were normalized to the control (100%).

Single Bacteria Evaluation without/with FA NP Treatment. The planktonic bacteria (OD = 0.1) were co-incubated without/with 250 μg/mL FA NPs in TSB or PBS medium for 6 h. Then the bacteria were washed with PBS three times for further analysis as follows:

DLS Analysis. The size and zeta potential were measured with DLS.

TEM Observation. The planktonic bacteria were fixed and dehydrated with an ethanol gradient series: 50%, 60%, 70%, 80%, 90%, 96%, and 100% ethanol aqueous solution, for 10 min each time. Then the bacteria were separated and loaded onto a carbon film-supported copper mesh for TEM analysis.

Co-localization Analysis. The planktonic bacteria were co-incubated without/with 50 μg/mL NR@FA NPs in TSB for 6 h. Then, the bacteria were washed with PBS and subsequently stained with 15 μg/mL WGA dye for 30 min. After washing with PBS, the bacteria were observed by CLSM under a 100× oil lens.

Competitive Inhibition. The peptidoglycan-targeting effect of FA NPs was studied by using two small-molecule inhibitors. Vancomycin and flavomycin are used as transpeptidation and transglycosylation inhibitors, respectively, to change the homeostasis of the cell wall at subtoxic concentrations. First, the MICs of inhibitors, vancomycin and flavomycin, against the bacteria were tested. Then, the bacteria were added to the TSB medium (1:100) containing these inhibitors at sub-MIC concentrations (0.25 and 0.5 × MIC) and allowed to grow for 1 h at 37 °C with shaking. Subsequently, to the mixture solution was added 50 μg/mL of NR@FA NPs and incubated for another 6 h. After that, the bacteria were washed with saline, followed by fixation with 4% paraformaldehyde for 20 min at room temperature. The cells were washed once more to remove paraformaldehyde with saline and analyzed by using a CytoFLEX LX flow cytometer.

In Vivo Subcutaneously Implanted Catheter Biofilm Infection Model. Female BALB/c mice (8 weeks old, 20 g) were purchased from Beijing Charles River Co., Ltd. The animals were treated and cared for under the National Research Council's Guide for the Care and Use of Laboratory Animals and under the supervision and assessment by the SPF Animal Department of Clinical Institute in China-Japan Friendship Hospital (Approval No. zryhyy 12-20-08-3). The subcutaneous implant catheter biofilm infection model was established according to the literature.[47] In general, catheters were cut into 1 cm length segments and sterilized by 75% ethanol. Then sterilized catheters were incubated in 100 mL

of TSB medium containing 1×10^8 CFU mL^{-1} of *S. aureus* 6538p (ATCC) at 37 °C for 48 h (replace fresh medium after 24 h). The catheters rinsed by PBS were implanted in the inner thighs of mice through a tiny incision. After 3 days, all the mice were randomly divided into four groups: PBS, FA NPs, Sita, and Sita@FA NPs, respectively. Drugs were injected subcutaneously into the infectious sites, including the interior and surrounding areas of the implanted catheters. For "twice", administration (2 mg/kg Sita each time) occurred two times, on day 3 and day 5. The mice were euthanized on day 7. For "once", one single administration (5 mg/kg Sita) was done on day 3. The mice were euthanized on day 10. After euthanasia, the implanted catheters were collected. The collected catheters were dispersed in PBS and sonicated for 10 min to make the bacteria fully detached into the suspension. Then, the suspension was diluted and spread on TSA plates for counting after a 24 h incubation at 37 °C in the incubator.

Data Analysis. Co-localization analysis and gap area calculation were performed using the ImageJ software. Statistical analyses were performed in GraphPad Prism 8.3.0 (GraphPad Software, USA). Quantitative data were expressed as mean ± SD. Statistically significant differences (p) between the two groups were analyzed by Student's t test. Statistically significant differences (p) between multigroups were analyzed by one- or two-way ANOVA with a Tukey test. ****$p < 0.0001$, ***$p < 0.001$, **$p < 0.01$, *$p < 0.05$, ns $p > 0.05$.

ASSOCIATED CONTENT

Ⓢ Supporting Information

The Supporting Information is available free of charge at https://pubs.acs.org/doi/10.1021/acsnano.3c10983.

Synthesis and characterizations of the polymers and the NPs; characterizations of the interaction between FA NPs and biofilm or between FA NPs and planktonic bacteria (PDF)

AUTHOR INFORMATION

Corresponding Authors

Guofeng Li − *State Key Laboratory of Organic−Inorganic Composites, Beijing Laboratory of Biomedical Materials, Beijing University of Chemical Technology, Beijing 100029, People's Republic of China;* ⓘ orcid.org/0000-0002-4101-0059; Email: ligf@mail.buct.edu.cn

Xing Wang − *State Key Laboratory of Organic−Inorganic Composites, Beijing Laboratory of Biomedical Materials, Beijing University of Chemical Technology, Beijing 100029, People's Republic of China;* ⓘ orcid.org/0000-0002-9990-1479; Email: wangxing@mail.buct.edu.cn

Thomas Fintan Moriarty − *AO Research Institute Davos, Davos 7270, Switzerland;* ⓘ orcid.org/0000-0003-2307-0397; Email: fintan.moriarty@aofoundation.org

Authors

Wenli Feng − *State Key Laboratory of Organic−Inorganic Composites, Beijing Laboratory of Biomedical Materials, Beijing University of Chemical Technology, Beijing 100029, People's Republic of China; AO Research Institute Davos, Davos 7270, Switzerland; China-Japan Friendship Hospital, Beijing 100029, People's Republic of China*

Marco Chittò − *AO Research Institute Davos, Davos 7270, Switzerland*

Wensheng Xie − *State Key Laboratory of Organic−Inorganic Composites, Beijing Laboratory of Biomedical Materials, Beijing University of Chemical Technology, Beijing 100029, People's Republic of China*

Qun Ren − *The Swiss Federal Laboratories for Materials Science and Technology, Laboratory for Biointerfaces, EMPA, 9014 St. Gallen, Switzerland;* ⓘ orcid.org/0000-0003-0627-761X

Fang Liu − *China-Japan Friendship Hospital, Beijing 100029, People's Republic of China*

Xiaoxu Kang − *State Key Laboratory of Organic−Inorganic Composites, Beijing Laboratory of Biomedical Materials, Beijing University of Chemical Technology, Beijing 100029, People's Republic of China*

Dongdong Zhao − *State Key Laboratory of Organic−Inorganic Composites, Beijing Laboratory of Biomedical Materials, Beijing University of Chemical Technology, Beijing 100029, People's Republic of China*

Complete contact information is available at:
https://pubs.acs.org/10.1021/acsnano.3c10983

Author Contributions

The manuscript was written through contributions of all authors. All authors have given approval to the final version of the manuscript. W.F., M.C., and W.X. contributed equally.

Notes

The authors declare no competing financial interest.

REFERENCES

(1) Masters, E. A.; Ricciardi, B. F.; Bentley, K. L. d. M.; Moriarty, T. F.; Schwarz, E. M.; Muthukrishnan, G. Skeletal infections: microbial pathogenesis, immunity and clinical management. *Nat. Rev. Microbiol* **2022**, *20* (7), 385−400.

(2) Arciola, C. R.; Campoccia, D.; Montanaro, L. Implant infections: adhesion, biofilm formation and immune evasion. *Nat. Rev. Microbiol* **2018**, *16* (7), 397−409.

(3) Kang, J.; Dietz, M. J.; Li, B. Antimicrobial peptide LL-37 is bactericidal against Staphylococcus aureus biofilms. *PLoS One* **2019**, *14* (6), No. e0216676.

(4) Flemming, H.-C.; van Hullebusch, E. D.; Neu, T. R.; Nielsen, P. H.; Seviour, T.; Stoodley, P.; Wingender, J.; Wuertz, S. The biofilm matrix: multitasking in a shared space. *Nat. Rev. Microbiol* **2023**, *21* (2), 70−86.

(5) Karygianni, L.; Ren, Z.; Koo, H.; Thurnheer, T. Biofilm Matrixome: Extracellular Components in Structured Microbial Communities. *Trends Microbiol.* **2020**, *28* (8), 668−681.

(6) Ciofu, O.; Moser, C.; Jensen, P. Ø.; Høiby, N. Tolerance and resistance of microbial biofilms. *Nat. Rev. Microbiol* **2022**, *20* (10), 621−635.

(7) Yan, J.; Bassler, B. L. Surviving as a community: antibiotic tolerance and persistence in bacterial biofilms. *Cell Host Microb* **2019**, *26* (1), 15−21.

(8) Xiao, X.; Zhang, S.; Chen, S.; Qian, Y.; Xie, J.; Cong, Z.; Zhang, D.; Zou, J.; Zhang, W.; Ji, Z.; Cui, R.; Qiao, Z.; Jiang, W.; Dai, Y.; Wang, Y.; Shao, X.; Sun, Y.; Xia, J.; Fei, J.; Liu, R. An alpha/beta chimeric peptide molecular brush for eradicating MRSA biofilms and persister cells to mitigate antimicrobial resistance. *Biomater. Sci.* **2020**, *8* (24), 6883−6889.

(9) Trubenová, B.; Roizman, D.; Moter, A.; Rolff, J.; Regoes, R. R. Population genetics, biofilm recalcitrance, and antibiotic resistance evolution. *Trends Microbiol.* **2022**, *30* (9), 841−852.

(10) Jo, J.; Price-Whelan, A.; Dietrich, L. E. P. Gradients and consequences of heterogeneity in biofilms. *Nat. Rev. Microbiol* **2022**, *20* (10), 593−607.

(11) Chen, Y.; Gao, Y.; Huang, Y.; Jin, Q.; Ji, J. Inhibiting Quorum Sensing by Active Targeted pH-Sensitive Nanoparticles for Enhanced Antibiotic Therapy of Biofilm-Associated Bacterial Infections. *ACS Nano* **2023**, *17* (11), 10019−10032.

(12) Ilana Kolodkin-Gal, D. R.; Shugeng, Cao; Jon, Clardy; Roberto, Kolter; Richard, Losick D-Amino Acids Trigger Biofilm Disassembly. *Science* **2010**, *328* (5978), 627−629.

(13) Vahdati, S. N.; Behboudi, H.; Navasatli, S. A.; Tavakoli, S.; Safavi, M. New insights into the inhibitory roles and mechanisms of D-amino acids in bacterial biofilms in medicine, industry, and agriculture. *Microbiol. Res.* **2022**, *263*, 127107.

(14) Unsal, T.; Wang, D.; Kumseranee, S.; Punpruk, S.; Gu, T. D-Tyrosine enhancement of microbiocide mitigation of carbon steel corrosion by a sulfate reducing bacterium biofilm. *World J. Microbiol. Biotechnol.* **2021**, *37* (6), 103.

(15) Li, Y.; Wuermanbieke, S.; Zhang, X.; Mu, W.; Ma, H.; Qi, F.; Sun, X.; Amat, A.; Cao, L. Effects of intra-articular D-amino acids combined with systemic vancomycin on an experimental Staphylococcus aureus-induced periprosthetic joint infection. *Journal of Microbiology, Immunology and Infection* **2022**, *55* (4), 716−727.

(16) Warraich, A. A.; Mohammed, A. R.; Perrie, Y.; Hussain, M.; Gibson, H.; Rahman, A. Evaluation of anti-biofilm activity of acidic amino acids and synergy with ciprofloxacin on Staphylococcus aureus biofilms. *Sci. Rep* **2020**, *10* (1), DOI: 10.1038/s41598-020-66082-x.

(17) Aliashkevich, A.; Alvarez, L.; Cava, F. New Insights Into the Mechanisms and Biological Roles of D-Amino Acids in Complex Eco-Systems. *Front. Microbiol.* **2018**, *9*, 683.

(18) Rubino, F. A.; Mollo, A.; Kumar, S.; Butler, E. K.; Ruiz, N.; Walker, S.; Kahne, D. E. Detection of Transport Intermediates in the Peptidoglycan Flippase MurJ Identifies Residues Essential for Conformational Cycling. *J. Am. Chem. Soc.* **2020**, *142* (12), 5482−5486.

(19) Oppenheimer-Shaanan, Y.; Steinberg, N.; Kolodkin-Gal, I. Small molecules are natural triggers for the disassembly of biofilms. *Trends Microbiol.* **2013**, *21* (11), 594−601.

(20) Milbrandt, N. B.; Tsai, Y. H.; Cui, K.; Ngompe Massado, C. S.; Jung, H.; Visperas, A.; Klika, A.; Piuzzi, N.; Higuera-Rueda, C. A.; Samia, A. C. S. Combination d-Amino Acid and Photothermal Hydrogel for the Treatment of Prosthetic Joint Infections. *ACS Applied Bio Materials* **2023**, *6* (3), 1231−1241.

(21) Fan, Q.; Wang, C.; Guo, R.; Jiang, X.; Li, W.; Chen, X.; Li, K.; Hong, W. Step-by-step dual stimuli-responsive nanoparticles for efficient bacterial biofilm eradication. *Biomater. Sci.* **2021**, *9* (20), 6889−6902.

(22) Sanchez, C. J.; Prieto, E. M.; Krueger, C. A.; Zienkiewicz, K. J.; Romano, D. R.; Ward, C. L.; Akers, K. S.; Guelcher, S. A.; Wenke, J. C. Effects of local delivery of d-amino acids from biofilm-dispersive scaffolds on infection in contaminated rat segmental defects. *Biomaterials* **2013**, *34* (30), 7533−7543.

(23) Wei, W.; Bing, W.; Ren, J.; Qu, X. Near infrared-caged d-amino acids multifunctional assembly for simultaneously eradicating biofilms and bacteria. *Chem. Commun.* **2015**, *51* (63), 12677−12679.

(24) Chen, M.; Zhang, S.; He, Z. Controlled Block Polypeptide Composed of d-Type Amino Acids: A Therapeutics Delivery Platform to Inhibit Biofilm Formation of Drug-Resistant Bacteria. *ACS Appl. Bio Mater.* **2020**, *3* (9), 6343−6350.

(25) Feng, W.; Huang, Z.; Kang, X.; Zhao, D.; Li, H.; Li, G.; Xu, J.; Wang, X. Self-Assembled Nanosized Vehicles from Amino Acid-Based Amphiphilic Polymers with Pendent Carboxyl Groups for Efficient Drug Delivery. *Biomacromolecules* **2021**, *22* (11), 4871−4882.

(26) Wang, T.; Cornel, E. J.; Li, C.; Du, J. Drug delivery approaches for enhanced antibiofilm therapy. *J. Controlled Release* **2023**, *353*, 350−365.

(27) Qi, G.; Hu, F.; Kenry; Chong, K. C.; Wu, M.; Gan, Y. H.; Liu, B. Bacterium-Templated Polymer for Self-Selective Ablation of Multidrug-Resistant Bacteria. *Adv. Funct. Mater.* **2020**, *30* (31), 2001338.

(28) Wang, Y.; Jiang, J.; Gao, Y.; Sun, Y.; Dai, J.; Wu, Y.; Qu, D.; Ma, G.; Fang, X. Staphylococcus epidermidis small basic protein (Sbp) forms amyloid fibrils, consistent with its function as a scaffolding protein in biofilms. *J. Biol. Chem.* **2018**, *293* (37), 14296−14311.

(29) Pletzer, D.; Hancock, R. E. W. Antibiofilm Peptides: Potential as Broad-Spectrum Agents. *J. Bacteriol.* **2016**, *198* (19), 2572−2578.

(30) Chen, X.; Xu, Y. Structural insights into assembly of transcription preinitiation complex. *Curr. Opin. Struct. Biol.* **2022**, *75*, 102404.

(31) Akbey, D. C.; Andreasen, M. Functional amyloids from bacterial biofilms-structural properties and interaction partners. *Chem. Sci.* **2022**, *13* (22), 6457−6477.

(32) Tian, S.; van der Mei, H. C.; Ren, Y.; Busscher, H. J.; Shi, L. Co-Delivery of an Amyloid-Disassembling Polyphenol Cross-Linked in a Micellar Shell with Core-Loaded Antibiotics for Balanced Biofilm Dispersal and Killing. *Adv. Funct. Mater.* **2022**, *32* (51), 2209185.

(33) Steinberg, N.; Keren-Paz, A.; Hou, Q.; Doron, S.; Yanuka-Golub, K.; Olender, T.; Hadar, R.; Rosenberg, G.; Jain, R.; Cámara-Almirón, J.; Romero, D.; van Teeffelen, S.; Kolodkin-Gal, I. The extracellular matrix protein TasA is a developmental cue that maintains a motile subpopulation within Bacillus subtilis biofilms. *Sci. Signal.* **2020**, *13* (632), No. eaaw8905.

(34) Mamou, G.; Corona, F.; Cohen-Khait, R.; Housden, N. G.; Yeung, V.; Sun, D.; Sridhar, P.; Pazos, M.; Knowles, T. J.; Kleanthous, C.; Vollmer, W. Peptidoglycan maturation controls outer membrane protein assembly. *Nature* **2022**, *606* (7916), 953−959.

(35) Feng, W.; Li, G.; Kang, X.; Wang, R.; Liu, F.; Zhao, D.; Li, H.; Bu, F.; Yu, Y.; Moriarty, T. F.; Ren, Q.; Wang, X. Cascade-Targeting Poly(amino acid) Nanoparticles Eliminate Intracellular Bacteria via On-Site Antibiotic Delivery. *Adv. Mater.* **2022**, *32*, 2109789.

(36) Lam, H.; Oh, D.-C.; Cava, F.; Takacs, C. N.; Clardy, J.; de Pedro, M. A.; Waldor, M. K. D-Amino Acids Govern Stationary Phase Cell Wall Remodeling in Bacteria. *Science* **2009**, *325* (5947), 1552−1555.

(37) Qiao, Y.; Lebar, M. D.; Schirner, K.; Schaefer, K.; Tsukamoto, H.; Kahne, D.; Walker, S. Detection of Lipid-Linked Peptidoglycan Precursors by Exploiting an Unexpected Transpeptidase Reaction. *J. Am. Chem. Soc.* **2014**, *136* (42), 14678−14681.

(38) Gautam, S.; Kim, T.; Shoda, T.; Sen, S.; Deep, D.; Luthra, R.; Ferreira, M. T.; Pinho, M. G.; Spiegel, D. A. An Activity-Based Probe for Studying Crosslinking in Live Bacteria. *Angew. Chem., Int. Ed.* **2015**, *127* (36), 10638−10642.

(39) Driks, A. Tapping into the biofilm: insights into assembly and disassembly of a novel amyloid fibre in Bacillus subtilis. *Mol. Microbiol.* **2011**, *80* (5), 1133−1136.

(40) Monteiro, J. M.; Fernandes, P. B.; Vaz, F.; Pereira, A. R.; Tavares, A. C.; Ferreira, M. T.; Pereira, P. M.; Veiga, H.; Kuru, E.; VanNieuwenhze, M. S.; Brun, Y. V.; Filipe, S. R.; Pinho, M. G. Cell shape dynamics during the staphylococcal cell cycle. *Nat. Commun.* **2015**, *6* (1), 8055.

(41) Monteiro, J. M.; Covas, G.; Rausch, D.; Filipe, S. R.; Schneider, T.; Sahl, H.-G.; Pinho, M. G. The pentaglycine bridges of Staphylococcus aureus peptidoglycan are essential for cell integrity. *Sci. Rep.* **2019**, *9* (1), 5010.

(42) Bucher, T.; Oppenheimer-Shaanan, Y.; Savidor, A.; Bloom-Ackermann, Z.; Kolodkin-Gal, I. Disturbance of the bacterial cell wall specifically interferes with biofilm formation. *Environ. Microbiol. Rep.* **2015**, *7* (6), 990−1004.

(43) Pidgeon, S. E.; Pires, M. M. Vancomycin-Dependent Response in Live Drug-Resistant Bacteria by Metabolic Labeling. *Angew. Chem., Int. Ed.* **2017**, *56* (30), 8839−8843.

(44) Liu, C.; Niu, J.; Cui, T.; Ren, J.; Qu, X. A Motor-Based Carbonaceous Nanocalabash Catalyst for Deep-Layered Bioorthogonal Chemistry. *J. Am. Chem. Soc.* **2022**, *144* (42), 19611−19618.

(45) Chou, S.; Guo, H.; Zingl, F. G.; Zhang, S.; Toska, J.; Xu, B.; Chen, Y.; Chen, P.; Waldor, M. K.; Zhao, W.; Mekalanos, J. J.; Mou, X. Synthetic peptides that form nanostructured micelles have potent antibiotic and antibiofilm activity against polymicrobial infections. *Proc. Natl. Acad. Sci. U. S. A.* **2023**, *120* (4), No. e2219679120.

(46) Li, G.; Feng, W.; Corrigan, N.; Boyer, C.; Wang, X.; Xu, J. Precise synthesis of poly(*N*-acryloyl amino acid) through photo-induced living polymerization. *Polym. Chem.* **2018**, *9*, 2733−2745.

(47) Li, P.; Chen, X.; Shen, Y.; Li, H.; Zou, Y.; Yuan, G.; Hu, P.; Hu, H. Mucus penetration enhanced lipid polymer nanoparticles improve the eradication rate of Helicobacter pylori biofilm. *J. Controlled Release* **2019**, *300*, 52−63.